Chemical and Structural Disorder in Eumelanins: A Possible Explanation for Broadband Absorbance

M. Linh Tran,* Ben J. Powell,† and Paul Meredith*
*Soft Condensed Matter Physics Group, and †Theoretical Condensed Matter Physics Group, School of Physical Sciences, University of Queensland, Brisbane, QLD 4072, Australia

ABSTRACT We report the results of an experimental and theoretical study of the electronic and structural properties of a key eumelanin precursor—5,6,-dihydroxyindole-2-carboxylic acid (DHICA)—and its dimeric forms. We have used optical spectroscopy to follow the oxidative polymerization of DHICA to eumelanin and observe red shifting and broadening of the absorption spectrum as the reaction proceeds. First principles density functional theory calculations indicate that DHICA oligomers (possible reaction products of oxidative polymerization) have the gap between the highest occupied molecular orbital and the lowest unoccupied molecular orbital red-shifted gaps with respect to the monomer. Furthermore, different bonding configurations (leading to oligomers with different structures) produce a range of gaps. These experimental and theoretical results lend support to the chemical disorder model where the broadband monotonic absorption characteristic of all melanins is a consequence of the superposition of a large number of nonhomogeneously broadened Gaussian transitions associated with each of the components of a melanin ensemble. These results suggest that the traditional model of eumelanin as an amorphous organic semiconductor is not required to explain its optical properties and should be thoroughly reexamined. These results have significant implications for our understanding of the physics, chemistry, and biological function of these important biological macromolecules. Indeed, one may speculate that the robust functionality of melanins in vitro is a direct consequence of its heterogeneity, i.e., chemical disorder is a "low cost" natural resource in these systems.

INTRODUCTION

The melanins are a broad class of functional macromolecule found throughout nature (1). In humans they serve as our primary photoprotectant in the hair, skin, and eyes, but they are also found in the inner ear and brain stem, where their roles are unclear (2). Pheomelanin (a brown-red pigment derived from cysteinyl-dopa) and eumelanin (a brown-black pigment formed from the oxidative polymerization of dihydroxyindolequinones) are the predominant forms in humans. Eumelanin is the more prevalent melanin pigment and has long been thought to be synthesized in vitro from tyrosine via the Raper-Mason enzymatic pathway (3,4). To date, biochemical and biophysical research has primarily focused on understanding the basic photochemistry, photobiology, and photophysics of these important substances and has been stimulated by the key role that melanins play in photoprotection and their potential involvement in the development of melanoma skin cancer (2). In addition to this biologically directed research, melanins have also attracted interest from molecular biophysicists (5–7), quantum chemists (8–15), and more recently, the functional materials and condensed matter physics communities (16) due to their rather unique physiochemical properties. Melanins exhibit broadband absorbance in the ultraviolet (UV) and visible (Fig. 1) and conduct electricity in the condensed phase (17,18). They have also been shown to photoconduct (19) and have a strong relative humidity-dependent conductivity at room temperature (20). Additionally, and consistent with its role as a photoprotectant, eumelanin has been shown to efficiently deactivate UV and visible photon energy, with radiative quantum yields of $<0.05\%$ (21). Such properties have led to the proposition that melanins may be of some use as biomimetic functional soft solids (16,22) in applications such as photovoltaics, gas sensing, and photothermal detectors. The prevailing paradigm is that melanins (eumelanin in particular) are condensed-phase organic semiconductors and that the broadband absorption (and indeed other electronic properties) can be explained by invoking a band structure model characteristic of an amorphous solid (17,23). Despite extensive experimental studies conducted on both natural and synthetic melanins, the structure, composition, and aggregation behavior of these systems are not well understood. This is in part due to their adverse chemical and physical properties such as low solubility in most common solvents (5,24), difficulty in separation by chromatography, and opacity. At the primary structural level, it is fairly well accepted that eumelanins (the brown-black type of melanin and the system of interest in this work) are macromolecules of the various redox forms of 5,6-dihydroxyindole-2-carboxylic acid (DHICA, 1a) and/or 5,6-dihydroxyindole (DHI, 1b) (Fig. 2) (1). These redox forms include DHI, quinone-imine (QI), and indolequinone (IQ) species (10,14). However, opinions as to the appropriate model at the secondary structural level remain divided. (Note, in this work we will use the

Submitted June 19, 2005, and accepted for publication September 26, 2005.

Address reprint requests to Paul Meredith, Soft Condensed Matter Physics Group, School of Physical Sciences, University of Queensland, Brisbane, QLD 4072, Australia. E-mail: meredith@physics.uq.edu.au.

M. Linh Tran's present address is School of Chemistry, University of Bristol, Cantock's Close, Bristol BS8 1TS, UK.

0006-3495/06/02/743/10 $2.00

doi: 10.1529/biophysj.105.069096

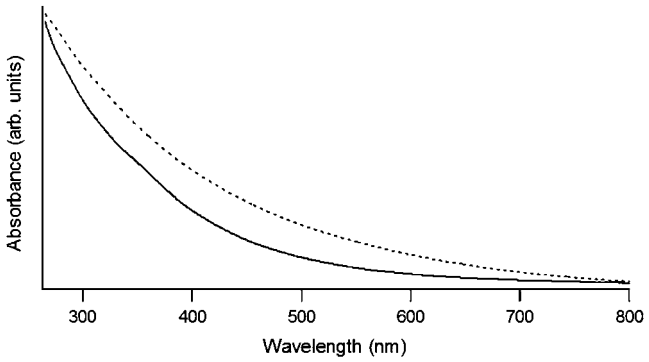

FIGURE 1 Characteristic broadband absorbance of eumelanin (*dashed line*) and pheomelanin (*solid line*). The spectra are featureless from the UV to the near infra-red and are more characteristic of an inorganic semiconductor than an organic pigment.

phrase ''secondary structure'' to refer to the supramolecular assembly of monomers in a nomenclature borrowed from proteins.) Historically, eumelanin has been viewed as a highly conjugated, spatially extended homo- or heteropolymer (23,25). However, in recent times, based primarily on a small number of x-ray scattering experiments (26) and attendant simulations, it has been proposed that eumelanin consists of small oligomeric units (<10 monomers) condensed by π-stacking into 4 or 5 oligomer nanoaggregates (26–29). This proposition requires a nanometer-sized protomolecule (the secondary structure) composed of sheets of covalently bonded DHI/DHICA monomers (with lateral extents of 15–20 Å). These protomolecules might then be stacked with ~3.4 Å intersheet spacing in a ''graphitic-like structure'' to form the aggregate. There remains some debate as to which model is appropriate.

Computational tools (ab initio and semiempirical) have also been used to shed light on this structural question. Following the pioneering studies of Galvao and Caldas (10), notable works by Bolivar-Martinez et al. (11), Bochenek and Gudowska-Nowak (12), Ill'ichev and Simon (13), Stark et al., (14,15), and the current authors (8,9) have attempted to provide corroborative evidence for the oligomeric model by calculating the structure and electronic properties of DHI monomers and associated small (2–6 monomer) oligomers. Our calculations using density functional theory (DFT) on both DHI and DHICA have shown that different redox states possess different HOMO-LUMO gaps (the energy difference between the highest occupied molecular orbital and the lowest unoccupied molecular orbital) (8,9). Several authors (8,9,12,14,15) have suggested that the broad absorption may be due to the overlapping absorption features of a large number of individual, chemically distinct species that constitute the heterogeneous eumelanin ensemble. This model, based upon what we term as ''chemical disorder'' (30), is an intriguing proposition, but, along with the oligomeric structural model, requires experimental proof.

Natural melanin is composed of a combination of DHI and DHICA with great variability in the amount of these two precursors in the macroscopic pigment (3,4,31). In this context, it is useful to prepare synthetically pure DHI and

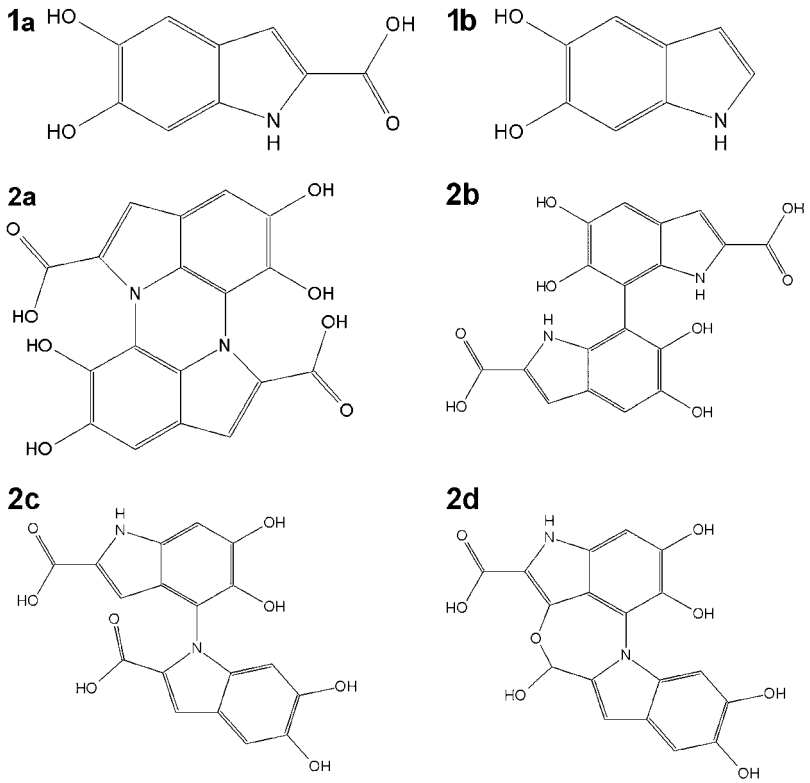

FIGURE 2 Schematic representation of DHICA (*1a*), DHI (*1b*), and the four dimers (*2a–2d*), which we also consider here.

DHICA monomers and monitor the formation of larger molecules as oxidative polymerization proceeds. The carboxylated form of the monomer is significantly easier to work with since DHI tends to spontaneously react under even the mildest conditions. In this study we use DHICA as our model ''eumelanin precursor''. We report its synthesis and detailed chemical characterization and use UV-visible spectroscopy and DFT as tools to understand how the electronic structure of the reaction products evolve during oxidative polymerization. Our data suggest that an amorphous organic semiconductor model is not required to explain the broadband absorbance of eumelanin, i.e., our data are consistent with the ''chemical disorder'' model. We believe it to be the first experimental evidence in support of this ''chemical disorder'' theory.

MATERIALS AND METHODS

Materials

DL-3,4-dihydroxyphenylalanine (DL-dopa) and potassium ferricyanide were purchased from Sigma Aldrich (Sydney, Australia). All other chemicals were of analytical grade. Milli-Q water (Millipore, Bedford, MA) (resistance, 18 MΩ.cm) was used throughout the experiments.

Synthesis of DHICA

The synthesis of DHICA was adapted from a procedure reported in the literature (32). Potassium ferricyanide solution (7 g, 3.04 mmol) in 60 mL water was added dropwise to a stirred solution of DL-dopa (1 g, 5.07 mmol) in 500 mL of water under a nitrogen atmosphere in a glovebox for 5 min, and then the mixture was allowed to stir for 8 min. A saturated solution of sodium sulfate was then added to the mixture to terminate the reaction, and the solution was allowed to stir for a further 8 min. The mixture was acidified to pH 2 using 6 M HCl and stirred for 10 min. The product was then extracted in ethyl acetate (~500 mL). The ethyl acetate portion was then washed with saturated sodium chloride solution twice, followed by a single wash with water. While under nitrogen, the ethyl acetate extract was transferred to a rotary evaporator and the solution was concentrated under vacuum. The reaction flask was then filled with nitrogen and transferred back into the glovebox. Hexane was added to precipitate the product, which was collected by vacuum filtration. The product was purple-gray in color (this is impurity-related color): m.p 220°C; EI-MS: m/z calculated for $C_9H_7NO_4$ (M^+) 193.15, found 193; analytical calculation for $C_9H_7NO_4$: C, 53.95; H, 3.85; N, 6.53, found: C, 53.81; H, 3.87; N, 6.53%. λ_{max} (DMSO) = 320 nm.

UV-visible kinetic experiments

The oxidation of DHICA in slightly basic (pH ~9) solution was followed using a PerkinElmer (Foster City, CA) λ40 UV-visible spectrometer. Absorption spectra 200–600 nm were recorded at a scan rate of 240 nm/min using a slit width of 4 nm and spectral resolution of 4 nm. Spectra were collected using a quartz 1 cm cuvette. Aliquots from a 2 mM solution were examined at time intervals of 0, 0.5, 1, 2, 4, 8, 12, 24, 51, and 74 h.

Instrumentation (NMR and x-ray photoelectron spectroscopy)

^{1}H and ^{13}C NMR spectra were run using a Bruker (Karlsruhe, Germany) DRX-500 high-resolution NMR spectrometer interfaced to an 11.7 Tesla 51 mm bore magnet system. DMSO-d6 was used as the solvent. X-ray photoelectron spectroscopy spectra were acquired with a Kratos Axis (Chesnut Ridge, NY) ULTRA X-ray Photoelectron Spectrometer incorporating a 165 nm hemispherical electron energy analyzer. The incident radiation was monochromatic Al K_α x-rays (1486.6 eV) at 150 W (15 kV, 10 mA). Survey (wide) scans were taken in the range of 0–1100 eV at a pass energy of 160 eV, and multiplex (narrow) high resolution scans were taken with a pass energy of 20 eV. Base pressure in the analysis chamber was 10^{-9} Torr during sample analysis. The DHICA powder was packed thickly onto a piece of black carbon tape.

The XPS spectral envelopes were resolved into component peaks using Gaussian-Lorentzian (10%–20% Lorentzian) curves. The binding energy (BE) of the spectra was referenced by assigning the main C*1s* hydrocarbon peak to 284.7 eV (33).

Calculation details

The chemical and electronic structures were calculated from first principles DFT. We performed our calculations using the Naval Research Laboratory Molecular Orbital Library (NRLMOL) (34–40). NRLMOL performs massively parallel electronic structure calculation using Gaussian orbital methods. Throughout we have used the Perdew, Burke, and Ernzerhof (PBE) (41) exchange correlation functional, which is a generalized gradient approximation (GGA) containing no free parameters. For each molecule we have fully relaxed the geometry with no symmetry constraints.

To calculate the structure of a molecule within DFT two nested problems must be solved self-consistently. First, one solves the self-consistent field (SCF) problem, which amounts to solving the Kohn-Sham equations within the Born-Oppenheimer approximation for a fixed set of nuclear coordinates. Second, the Hellman-Feynman theorem is used to calculate the forces on the nuclei and thus iteratively search for a local minimum of the energy in the space of structures. In any self-consistent solution, criteria must be chosen to allow one to decide when the problem is converged. In this work we consider the SCF problem to be converged when successive iterations differ in total energy by $<10^{-8}$ Ha and geometries to be converged when the largest force acting on any atom are $<10^{-3}$ Ha/Bohr.

In all of the calculations presented in this work we use Porezag-Pederson (PP) basis sets (42), which, in contrast to standard approaches, are not fixed sets of basis functions, but are adjusted based on a total-energy criterion. PP basis sets have been proven to satisfy the $Z^{10/3}$ theorem and, for weakly interacting atoms, it has been shown that PP basis sets have no superposition error (43). These basis sets are available on request.

DFT is a theory of the ground state; therefore calculations represent the energy gap between Kohn-Sham eigenvalues and not the true HOMO-LUMO gap of the molecules. This is known as the band gap problem (44). Therefore we have also employed the ΔSCF method (44) to calculate the HOMO-LUMO gap. We have previously shown that equivalent results for DHI reproduce the trends found in time-dependent DFT calculations (8).

RESULTS AND DISCUSSION

Characterization of DHICA

Several single-step synthetic approaches to DHICA have been published (32,45,46). For the research reported here, a modification of Kroesche's method was used. The ^{1}H NMR spectrum of DHICA (Fig. 3) revealed broad resonances at 8.59 and 9.10 ppm associated with the hydroxy groups in the 5 and 6 positions. Another important feature is the 11.13 ppm peak assigned to the indole amine proton. Finally the carboxylic acid proton broadband appears at 12.31 ppm. The other resonances corresponding to the aromatic ring protons

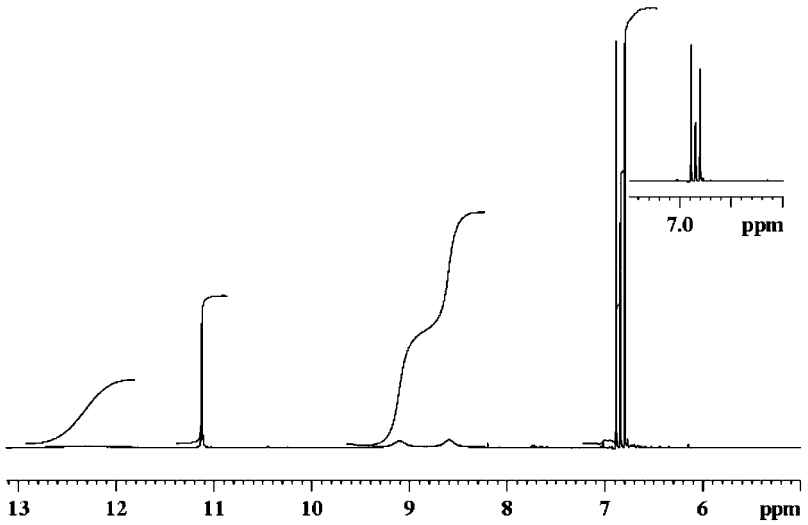

FIGURE 3 ^{1}H NMR of DHICA in DMSO-d6.

at 6.89, 6.85, and 6.77 ppm also appear. The values for the ^{1}H NMR peaks are in close agreement with literature reports (32,47). The assignments for the ^{13}C NMR spectrum are shown in Table 1. Of significance are the signals for the –COOH moiety at 162.75 ppm and the –OH groups at 146.11 and 141.98 ppm. There was no observation of the presence of quinone in the ^{13}C NMR spectrum. To further establish that the hydroxy groups did not oxidize into quinone groups, the XPS spectra of DHICA were acquired and interpreted. The C *1s* spectral envelope contained components arising from the various functional groups found in DHICA (Fig. 5 *a*). The assignments for the components are presented in Table 2. The COOH group occurs at 288.7 eV, a BE shift of 4 eV from the main aromatic signal. The aromatic shake-up peaks can also be observed at higher binding energies to the COOH band. The only other peaks present were those due to the C-N or C-OH atoms and no C=O functionality was observed, suggesting conversion to the quinone form did not occur. The N *1s* and O *1s* spectra (Figs. 4 *c* and 5 *b*) provided corroborative evidence for the structure of DHICA. It was observed that only one type of nitrogen signal arose and it was assigned to the indole nitrogen group. In the O *1s* spectrum the area ratio of C-OH and C=O peaks at 533.53 and 531.86 eV, respectively (33), agreed with theoretical predictions of 3:1. The NMR and XPS spectra, along with the mass spectral information and microanalysis results reported in the experimental section, provide comprehensive characterization of the melanin precursor.

UV-visible experiments

The evolution of the DHICA monomer into larger ''eumelanin'' molecules was followed using UV-visible spectroscopy. Fig. 6 *a* shows the absorption spectrum of a weakly basic DHICA solution at the start of this experiment. Initially one prominent absorption peak appears centered at 328 nm corresponding to the lowest energy DHICA transition, which calculations show to be a $\pi-\pi^*$ transition (note that there is a node in the electron density in the plane of the molecule of the HOMOs and LUMOs reported in Powell (9)). Taking the HOMO-LUMO gap to correspond to the lowest energy transition, an experimental value for this gap of 3.8 eV can be extracted (which is consistent with the HOMO-LUMO gap of 3.0 eV calculated for a DHICA monomer in Powell (9), given the band gap problem discussed above and the fact that calculations neglect solvent effects (47), see below). This suggests that at this stage only the monomer is present in solution. Over time, the absorption maximum red shifts and the initial peak broadens (Fig. 6 *b*) in a progressive fashion until it almost disappears at the end of the monitoring time (74 h). This shift is likely to be a convolution effect as absorption by reaction

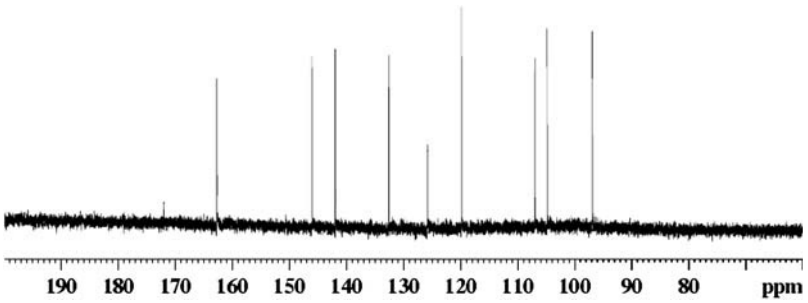

FIGURE 4 ^{13}C NMR of DHICA in DMSO-d6.

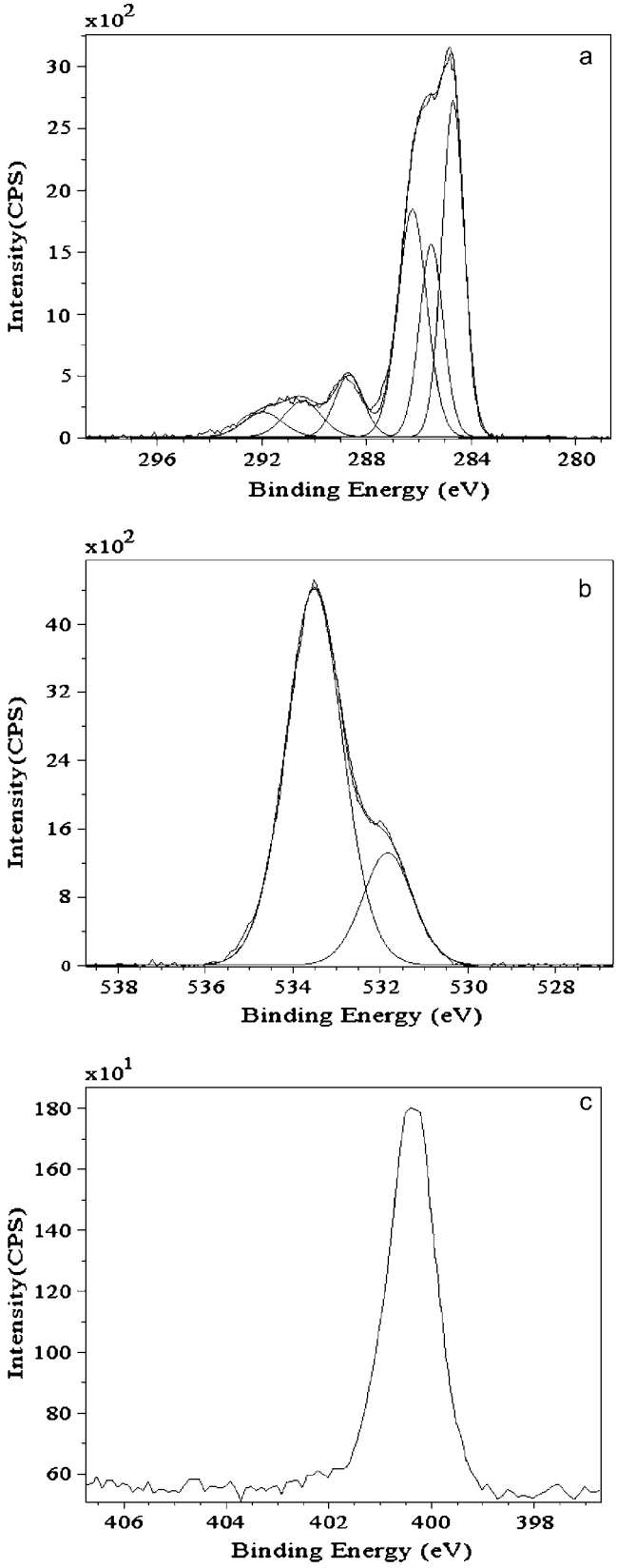

FIGURE 5 XPS spectra of DHICA. (*a*), C 1s region,(*b*), O 1s region, and (*c*) N 1s region. See text and Table 2 for assignments of individual components.

TABLE 1 ^{13}C NMR of DHICA in DMSO-d6, peak assignments (relative to those presented in Borges et al. (31))

Peak/ppm	Assignment	Literature
96.92	C7	97.29
104.87	C3	105.27
107.02	C4	107.43
119.86	C8	120.22
125.84	C2	126.13
132.60	C9	132.97
141.11	C6	142.32
146.11	C5	146.46
162.75	COOH	163.03

products (higher order species) at lower wavelengths smear out the initial 328 nm absorption maximum. The dramatic broadening of the absorption profile also offers evidence for the formation of reaction products with lower energy HOMO-LUMO gaps (see the dimer results in the next section). At the end stages, the absorption profile, although never becoming monotonic, approaches the broad spectrum characteristic of eumelanin solutions (48). It has previously been suggested that this broad absorbance observed in all melanins can be explained in terms of structural and chemical heterogeneity (30). In this ''chemical disorder'' model, melanin solutions (or indeed condensed phase films or powders) are ensembles containing a large range of chemically distinct macromolecules (oligomeric or polymeric), each with a different HOMO-LUMO gap. The exponential monotonic absorption is then a result of the superposition of a large number of nonhomogeneously broadened Gaussian transitions associated with each of the components of the ensemble. We have previously predicted that DHICA macromolecular ensembles contain less ''effective chemical disorder'' than the equivalent DHI macromolecular ensembles (9). This prediction is based upon the fact that the (oxidized) quinone forms of the DHICA monomer are energetically unstable and therefore not likely to form. This is not the case for DHI. The fact that the oxidative polymerization of DHICA does not lead to a truly monotonic profile is entirely consistent with this prediction, as is the fact that we do not see a quinone in the analysis of the monomer.

It has been suggested that scattering contributes significantly to measurements of melanin absorption (49). A broadening (50) of the spectrum into the visible would require Mie scattering from undissolved particles in solution. Several authors have shown that scattering is significant under

TABLE 2 XPS carbon *1s* peak positions for DHICA (from Fig. 5 *a*)

BE/eV	Assignment
284.69	C aromatics
285.55	C-N
286.26	C-O
288.66	C=O

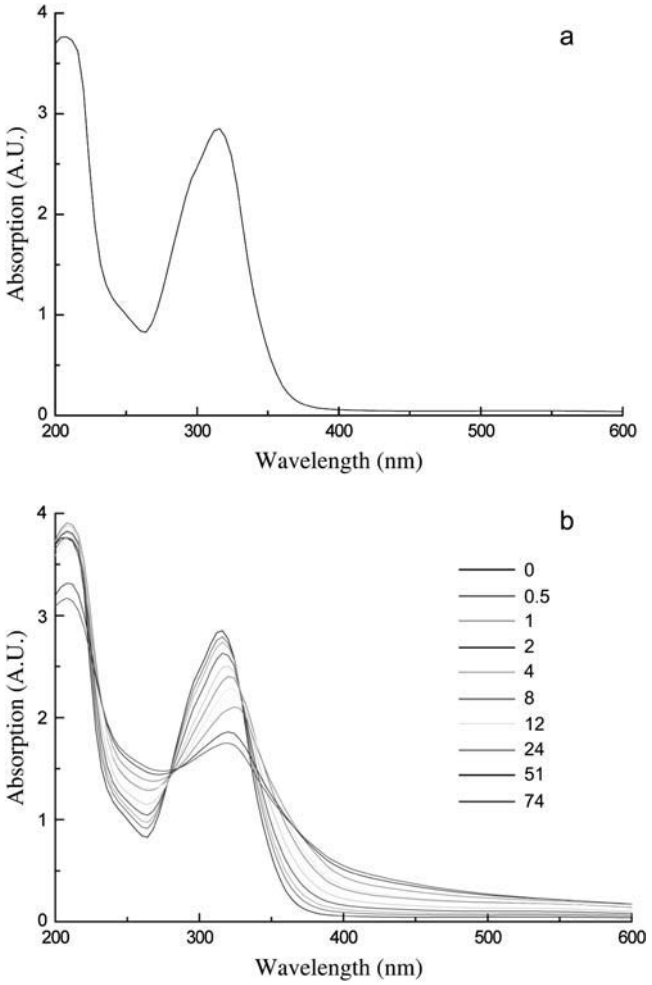

FIGURE 6 UV-visible absorption spectra DHICA in NaOH solution at $t = 0$ (*a*) and at various times (*b*) (legend represents hours).

specific conditions of neutral or low pH and high concentration, i.e., in the low solubility limit (51,52). The eumelanin solutions can even appear turbid and milky. In the study by Vitkin et al. (51), it was estimated that scattering contributed a maximum of 20% to the absorption coefficient. However, there is now a significant body of literature to confirm that the monotonically decreasing absorption with increasing wavelength in melanins is in fact due to ''real absorption'' (see, for example, Huang et al. (53) and Kurtz (54))—especially under the types of conditions we employ in our study: alkaline pH and low concentrations. We have also recently shown that working within this regime in combination with a mathematical procedure to account for excitation attenuation and emission reabsorption allows one to extract quantitative information from optical emission and excitation spectra of eumelanins (21,55).

The absorptions at 328 nm and 250 nm were examined more closely (Fig. 7). It was found that the absorption by the monomer precursor decreased linearly as a function of time. This result suggests that the consumption of DHICA molecules is constant. The absorption band at 250 nm progressively increases as the reaction proceeds. It is conceivable that this feature is associated with transitions to higher lying states in reaction products. The growth of these products is nonlinear as a function of time and was found to obey the relation:

$$conc. = \frac{b + ct}{1 + at}, \tag{1}$$

where b, c, and a are constants. Fitting the data to Eq. 1, the extracted values for the constant are as follows: $a = 0.152$ h^{-1}, $b = 1$ mol ltr^{-1}, $c = 0.25$ mol $ltr^{-1}h^{-1}$. In general, such complex kinetics indicates the presence of competing forward and backward reactions, whose rates are dependent upon the availability of precursor. It would also indicate that the reaction proceeds via a stable intermediate (for example, a small oligomeric species) which ceases to be the primary reaction product at a critical concentration of available reactant and becomes the building block for subsequent products. This idea of an oligomeric ''protomolecule'' is consistent with a heterogeneous ensemble picture.

Quantum chemical calculations

It has previously been shown (9) that, in vacuo, DHICA is significantly more stable than its oxidized forms (the quinone and semiquinone forms). We therefore restrict our attention to the 5,6-dihydroxy form, which is labeled as 1a in Fig. 2. Also shown in Fig. 2 are four possible dimers of DHICA (*2a–2d*). We study these molecules as a representative sample of the type of molecules that will form as a result of oxidative polymerization. Clearly this is not the complete set of all possible dimers, but our objective here is to examine the implications of polymerization with respect to the HOMO-LUMO gaps of the products. In Table 3, we report the total energy calculated for molecules 2a–2d relative to

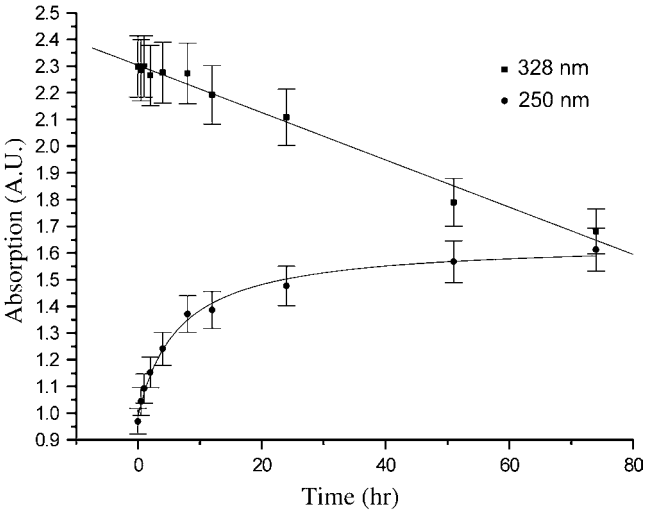

FIGURE 7 Absorption versus time plots of the DHICA solution at 328 nm and 250 nm.

twice that of 1a. We also calculate the relative abundances of these dimers at 300 K (Table 3), neglecting entropic effects. Here something of a puzzle emerges. Our calculations indicate that none of the dimers we have considered are stable with respect to two monomers in reactions such as 2a + $2H_2$ → 2(1a), i.e., they should not form. However, it is by no means clear that this represents the situation in the actual reaction mix. In particular, it is important to note that our calculations represent the situation in vacuo. The stability of the dimers may be somewhat different in a solvent—in particular the hydrogens given off in the reaction are unlikely to form H_2 (which indicates that we have significantly underestimated the enthalpy of the dimers relative to the monomer) and further solvent effects may significantly alter the relative enthalpy and, perhaps more significantly, the entropy associated with each molecule. For example, it has been previously predicted that significant hydrogen-bonded networks are formed around DHI monomers in an aqueous environment (8). It should also be noted that several stable dimers are known for DHI (Powell et al. (8) and references therein). We have therefore also reported the energy of vaporization per atom in Table 3. In contrast to the simple interpretation of the relative energies, this suggests that the dimers with two intermonomer bonds (2a and 2d) are stable with respect to those with a single intermonomer bond (2b and 2c) and that all of the dimers are stable with respect to the monomer. The claim that dimers with two intermonomer bonds are more stable than those with a single cross-link is consistent with the results of Stark et al. (14), who found that planarity had a significant effect in stabilizing dimers formed from IQ. However, the safest interpretation of the data presented in Table 3 is that it indicates that 2b is stable relative to 2c, and 2d is stable with respect to 2a, but that no conclusions can be safely drawn of the relative stabilities of the dimers and monomers. However, it is clear from Figs. 6 and 7 that the reactions moving from the monomer to the macromolecule is extremely slow, which may be what the apparent low enthalpy of the dimers is reflecting.

TABLE 3 Total energy (eV) and relative abundance of four possible dimers of DHICA (cf. Fig. 2)

Molecule	Total energy (eV)	Relative abundance in vacuo at 300 K	Energy of vaporization per atom (eV)
2a	3.82	$<10^{-32}$	1004.157
2b	1.96	1	957.511
2c	4.02	$<10^{-34}$	954.738
2d	2.89	$<10^{-15}$	1004.181

The total energies are quoted relative to twice the energy of 1a and are adjusted for chemical change by assuming that all of the removed hydrogens form H_2. The relative abundance is calculated assuming a Boltzmann distribution at 300 K. This naïve treatment of the calculated energies is probably inadequate. In particular, the energy of the hydrogen is likely to depend on the detailed chemistry of the solvent. Indeed, this probably means that it is not correct to compare the energies of 2a and 2d with those of 2b and 2c. Another way to estimate the relative stability of the molecules is to calculate the energy required to vaporize the molecule per atom. This is therefore also presented in the table. It can be seen that significantly more energy per atom is required to vaporize 2a and 2d than 2b or 2c, suggesting that the former are more stable. (Note that the equivalent figure for molecule 1a is 910.126 eV, suggesting that the dimers are, in fact, stable.) However, it is clear that 2d is significantly more stable than 2a and that 2b is significantly more stable than 2c.

In Table 4 we compare the HOMO-LUMO gap found from a simple interpretation of the Kohn-Sham eigenvalues with those found by the ΔSCF method for molecules 2a–2d. For comparison we reproduce the previously published (9) result for 1a in Table 4. Once again, we note that these calculations represent the in vacuo situation, and one would expect the presence of a polar solvent to nonhomogeneously broaden and shift these results (whether this is a red shift or a blue shift will depend, in general, on the details of the molecule-solvent interaction—but the direction and relative magnitude of the shift would be consistent for all molecules) (45). Despite this caveat, it is clear that the HOMO-LUMO gaps of all four dimers are significantly red shifted with respect to the monomer, i.e., even the lowest molecular weight reaction products will have absorption maxima at longer wavelengths than the original precursor (DHICA). One can clearly see why this red shifting occurs by examining the electronic densities of the HOMOs and LUMOs of molecules 2a–2d (Fig. 8). Significant electron density is distributed spatially over the entire molecule in all of the orbitals. This extended delocalization naturally corresponds to a reduction of the energy gap relative to the parent monomer. It can also be seen that 2a and 2d are further red shifted than 2b and 2c (cf. Table 4). This appears to be a direct result of the greater delocalization afforded by the fact that 2a and 2d have two intermonomer bonds rather than the single intermonomer bond found in 2b and 2c. This result is also consistent with the findings of Stark et al. who found that planarity led to a reduction of the HOMO-LUMO gap in dimers of QI (14). Furthermore, each dimer has a different gap value over a range of 0.2 eV. These are important results since they confirm that a simple ensemble containing the monomer and a relatively small number of dimers would indeed produce an absorption profile approaching that

TABLE 4 HOMO-LUMO gap (in eV) for the monomer (1a) (reproduced from Powell (9)) and four possible dimers (2a–2d)

Molecule	Simple interpretation of the Kohn-Sham eigenvalues	ΔSCF
1a	2.85 eV	3.04 eV (407 nm)
2a	2.02 eV	2.13 eV (581 nm)
2b	2.24 eV	2.32 eV (534 nm)
2c	2.28 eV	2.46 eV (504 nm)
2d	2.04 eV	2.26 eV (549 nm)

We compare the value found from the simple interpretation of the Kohn-Sham value, which tends to underestimate the HOMO-LUMO gap because of the band gap problem, with the results of ΔSCF calculations, which are known to be much more accurate (41). It has previously been shown (8) that, for DHI, ΔSCF calculations are in good agreement with time-dependent DFT calculations. All of the dimers show a significant red shift compared to the monomer.

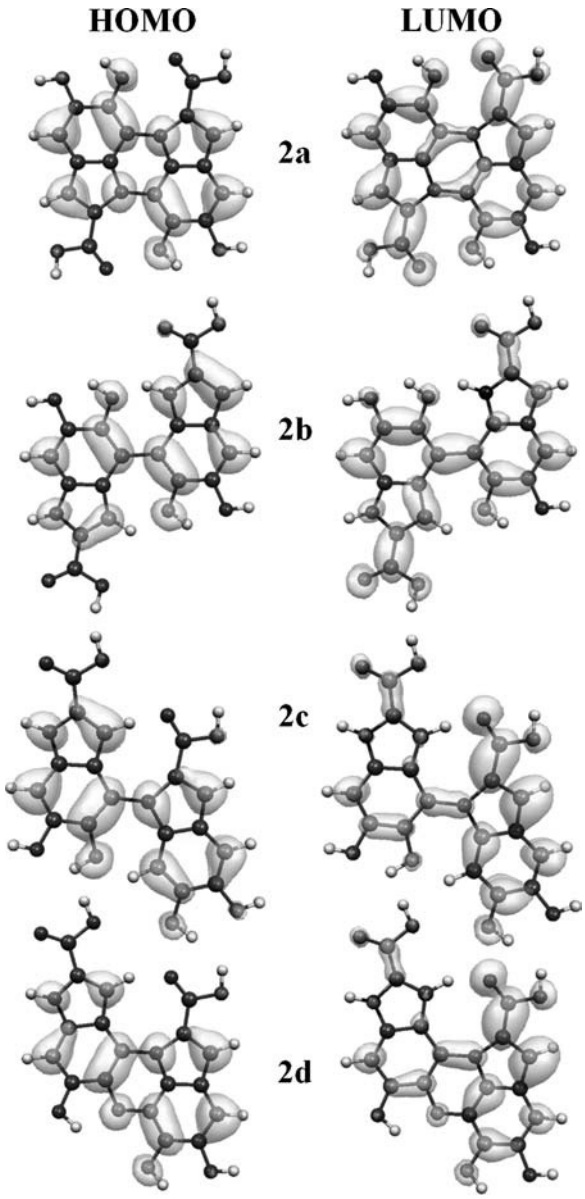

FIGURE 8 Electron density in the highest occupied molecular orbital (HOMO, *left*) and lowest unoccupied molecular orbital (LUMO, *right*) of 2a–d.

observed for the polymerized DHICA solutions. Based upon this analysis, widening the ensemble to include other monomer types (DHI and its oxidized forms as in real eumelanins), a greater range of dimers, and higher order oligomers (trimers, tetramers, etc. with further red-shifted HOMO-LUMO gaps) all with different abundances and absorption cross sections, would be expected to produce the characteristic melanin broadband monotonic absorption. Hence, the traditional extended homopolymer or heteropolymer organic semiconductor model is not required to explain the optical absorption of eumelanin. The secret to the robust functionality of these mysterious functional macromolecules may be associated with the extreme chemical disorder inherent in their secondary structure. If true, this new structural model has profound implications for our understanding of the physics and chemistry of melanins. In particular, the long held view that they are condensed phase semiconductors should be reexamined. Additionally, from the biological function perspective (melanins are the primary photoprotectants in humans) we should consider how these ensembles are capable of nearly complete deactivation of UV-visible photon energy. Finally, in a more generic sense, it may be interesting to speculate whether the rather ''low cost'' resource of chemical disorder is used elsewhere in nature to create robust electronic functionality (for example, coupling heterogeneity in the antenna chlorophylls of photo-system I of cyanobacteria is thought to red shift and broaden the antenna absorption cross section (56)) or whether the melanins are a unique case.

CONCLUSIONS

In this work, we have reported the synthesis of a stable and convenient eumelanin precursor, namely DHICA. This moiety is present in the natural and synthetic forms of eumelanin together with DHI and its reduced forms. We have used UV-visible spectroscopy to follow the oxidative polymerization of DHICA and observe red shifting and broadening of the absorption spectrum as the reaction proceeds. First principles density functional theory calculations indicate that DHICA oligomers (the likely reaction products of oxidative polymerization) have red shifted HOMO-LUMO gaps with respect to the monomer. Furthermore, different bonding configurations (leading to oligomers with different secondary structures) produce a range of gaps. These experimental and theoretical results lend support to the chemical disorder model where the broadband monotonic absorption is a consequence of the superposition of a large number of nonhomogeneously broadened Gaussian transitions associated with each of the components of the eumelanin ensemble. We therefore conclude that the traditional model of melanin as an amorphous organic semiconductor is not required to explain its optical properties, and should be thoroughly reexamined.

We thank Tunna Baruah, Noam Bernstein, Paul Burn, Joel Gilmore, Ross McKenzie, Mark Pederson, Jenny Riesz, Jeff Riemers, and Tad Sarna for enlightening discussions.

B.J.P. would like to express his gratitude to Ross McKenzie for financial support during this research. The work was funded by the Australian Research Council (Discovery Program), and calculations were performed at the Australian Partnership for Advanced Computing National Facility under a grant from the Merit Allocation Scheme.

REFERENCES

1. Prota, G. 1992. Melanins and Melanogenesis. Academic Press, San Diego, CA.
2. Zhang, X., C. Erb, J. Flammer, and W. M. Nau. 2000. Absolute rate constants for the quenching of reactive excited states by melanin and related 5,6-dihydroxyindole metabolites: implications for their antioxidant activity. *Photochem. Photobiol.* 71:524–533.

3. Ito, S. 1986. Reexamination of the structure of eumelanin. *Biochim. Biophys. Acta.* 883:155–161.
4. Tsukamoto, K., A. Palumbo, M. D'Ischia, V. J. Hearing, and G. Prota. 1992. 5,6-Dihydroxyindole-2-carboxylic acid is incorporated in mammalian melanin. *Biochem. J.* 286:491–495.
5. Sarna, T., B. Pilas, E. J. Land, and T. G. Truscott. 1986. Interaction of radicals from water radiolysis with melanin. *Biochim. Biophys. Acta.* 883:162–167.
6. Zajac, G. W., J. M. Gallas, J. Cheng, M. Eisner, S. C. Moss, and A. E. Alvarado-Swaisgood. 1994. The fundamental unit of synthetic melanin: a verification by tunneling microscopy of x-ray scattering results. *Biochim. Biophys. Acta.* 1199:271–278.
7. Gallas, J. M., G. W. Zajac, T. Sarna, and P. L. Stotter. 2000. Structural differences in unbleached and mildly bleached synthetic tyrosine-derived melanins identified by scanning probe microscopies. *Pigment Cell Res.* 13:99–108.
8. Powell, B. J., T. Baruah, N. Bernstein, K. Brake, R. H. McKenzie, P. Meredith, and M. R. Pederson. 2004. A first-principles density-functional calculation of the electronic and vibrational structure of the key melanin monomers. *J. Chem. Phys.* 120:8608–8615.
9. Powell, B. J. 2005. 5,6-Dihydroxyindole-2-carboxylic acid: a first principles density functional study. *Chem. Phys. Lett.* 402:111–115.
10. Galvão, D. S., and M. J. Caldas. 1988. Polymerization of 5,6-indolequinone: a view into the band structure of melanins. *J. Chem. Phys.* 88:4088–4091.
11. Bolivar-Marinez, L. E., D. S. Galvão, and M. J. Caldas. 1999. Geometric and spectroscopic study of some molecules related to eumelanins. 1. Monomers. *J. Phys. Chem. B.* 103:2993–3000.
12. Bochenek, K., and E. Gudowska-Nowak. 2003. Fundamental building blocks of eumelanins: electronic properties of indolequinone-dimers. *Chem. Phys. Lett.* 373:532–538.
13. Il'ichev, Y. V., and J. D. Simon. 2003. Building blocks of eumelanin: relative stability and excitation energies of tautomers of 5,6-dihydroxyindole and 5,6-indolequinone. *J. Phys. Chem. B.* 107:7162–7171.
14. Stark, K. B., J. M. Gallas, G. W. Zajac, M. Eisner, and J. T. Golab. 2003. Spectroscopic study and simulation from recent structural models for eumelanin: II. Oligomers. *J. Phys. Chem. B.* 107:11558–11562.
15. Stark, K. B., J. M. Gallas, G. W. Zajac, J. T. Golab, S. Gidanian, T. McIntire, and P. J. Farmer. 2005. Effect of stacking and redox state on optical absorption spectra of melanins—comparison of theoretical and experimental results. *J. Phys. Chem. B.* 109:1970–1977.
16. Meredith, P., B. J. Powell, J. Riesz, R. Vogel, D. Blake, I. Kartini, G. Will, and S. Subianto. 2005. Broadband photon-harvesting biomolecules for photovoltaics. *In* Artificial Photosynthesis: From Basic Biology to Industrial Application. A. F. Collings and C. Critchley, editors. Wiley-VCH, Weinheim, Germany. 37–64.
17. McGinnes, J., P. Corry, and P. Proctor. 1974. Amorphous-semiconductor switching in melanins. *Science.* 183:853–855.
18. Jastrzebska, M. M., H. Isotalo, J. Paloheimo, and H. Stubb. 1995. Electrical conductivity of synthetic DOPA-melanin polymer for different hydration states and temperatures. *J. Biomater. Sci. Polym. Ed.* 7:577–586.
19. Rosei, M. A., L. Mosca, and F. Galluzzi. 1996. Photoelectronic properties of synthetic melanins. *Synth. Met.* 76:331–335.
20. Giacomantonio, C. 2005. Change transport in melanin, a disordered bio-organic conductor. Honors Thesis. The University of Queensland, Brisbane, Australia.
21. Meredith, P., and J. Riesz. 2004. Radiative relaxation quantum yields for synthetic eumelanin. *Photochem. Photobiol.* 79:211–216.
22. Meredith, P. 2004. Components based on melanin and melanin-like bio-molecules, and process for their production. U.S. Patent US10/491224.
23. Longuet-Higgins, H. C. 1960. Origin of the free radical property of melanins. *Arch. Biochem. Biophys.* 88:231–232.
24. Ridente, Y., G. C. Azzellini, and A. S. Ito. 1993. Free radicals in melanin-cationic porphyrins complexes in the dark and under light irradiation. *Pigment Cell Res.* 6:134–139.
25. Pullman, A., and B. Pullman. 1961. The band structure of melanins. *Biochim. Biophys. Acta.* 54:384–385.
26. Gallas, J. M., K. C. Littrell, S. Seifert, G. W. Zajac, and P. Thiyagarajan. 1999. Solution structure of copper ion-induced molecular aggregates of tyrosine melanin. *Biophys. J.* 77:1135–1142.
27. Littrell, K. C., J. M. Gallas, G. W. Zajac, and P. Thiyagarajan. 2003. Structural studies of bleached melanin by synchrotron small-angle x-ray scattering. *Photochem. Photobiol.* 77:115–120.
28. Clancy, C. M. R., J. B. Nofsinger, R. K. Hanks, and J. D. Simon. 2000. A hierarchical self-assembly of eumelanin. *J. Phys. Chem. B.* 104: 7871–7873.
29. Clancy, C. M. R., and J. D. Simon. 2001. Ultrastructural organization of eumelanin from Sepia officinalis measured by atomic force microscopy. *Biochemistry.* 40:13353–13360.
30. Meredith, P., B. J. Powell, J. Riesz, S. Nighswander-Rempel, M. R. Pederson, and E. Moore. 2006. Towards structure-property-function relationships for eumelanin. *Soft Matter.* 2:37–44.
31. Borges, C. R., J. C. Roberts, D. G. Wilkins, and D. E. Rollins. 2001. Relationship of melanin degradation products to actual melanin content: application to human hair. *Anal. Biochem.* 290:116–125.
32. Kroesche, C., and M. G. Peter. 1996. Detection of melanochromes by MALDI-TOF mass spectrometry. *Tetrahedron.* 52:3947–3952.
33. Briggs, D. 1998. Surface Analysis of Polymers by XPS and Static SIMS. Cambridge University Press, Cambridge, U.K.
34. Pederson, M. R., and K. A. Jackson. 1990. Variational mesh for quantum-mechanical simulations. *Phys. Rev. B.* 41:7453–7461.
35. Jackson, K., and M. R. Pederson. 1990. Accurate forces in a local-orbital approach to the local-density approximation. *Phys. Rev. B.* 42: 3276–3281.
36. Pederson, M. R., and K. A. Jackson. 1991. Pseudoenergies for simulations on metallic systems. *Phys. Rev. B.* 43:7312–7315.
37. Quong, A. A., M. R. Pederson, and J. L. Feldman. 1993. First principles determination of the interatomic force-constant tensor of the fullerene molecule. *Solid State Commun.* 87:535–539.
38. Porezag, D., and M. R. Pederson. 1996. Infrared intensities and Raman-scattering activities within density-functional theory. *Phys. Rev. B.* 54:7830–7836.
39. Porezag, D. V. 1997. Development of ab-initio and approximate density functional methods and their application to complex fullerene systems. PhD thesis. Technische Universität, Chemnitz, Germany.
40. Briley, A., M. R. Pederson, K. A. Jackson, D. C. Patton, and D. V. Porezag. 1998. Vibrational frequencies and intensities of small molecules: all-electron, pseudopotential, and mixed-potential methodologies. *Phys. Rev. B.* 58:1786–1793.
41. Perdew, J. P., K. Burke, and M. Ernzerhof. 1996. Generalized gradient approximation made simple. *Phys. Rev. Lett.* 77:3865–3868.
42. Porezag, D., and M. R. Pederson. 1999. Optimization of Gaussian basis sets for density-functional calculations. *Phys. Rev. A.* 60:2840–2847.
43. Patton, D. C., and M. R. Pederson. 1997. Application of the generalized-gradient approximation to rare-gas dimers. *Phys. Rev. A.* 56:R2495–R2498.
44. Jones, R. O., and O. Gunnarsson. 1989. The density functional formalism, its applications and prospects. *Rev. Mod. Phys.* 61:689–746.
45. Beer, R. J. S., K. Clarke, H. G. Khorana, and A. Robertson. 1948. Chemistry of melanins. I. Synthesis of 5,6-dihydroxyindole and related compounds. *J. Chem. Soc.* Abstracts:2223–2226.
46. Beer, R. J. S., L. McGrath, A. Robertson, A. B. Woodier, and J. S. E. Halker. 1949. Chemistry of the melanins. II. The synthesis of 5,6-dihydroxy-2-indolecarboxylic acid and related compounds. *J. Chem. Soc.* Abstracts:2061–2066.

47. Pezzella, A., A. Napolitano, M. d'Ischia, and G. Prota. 1996. Oxidative polymerization of 5,6-dihydroxyindole-2-carboxylic acid to melanin: a new insight. *Tetrahedron.* 52:7913–7920.

48. Crippa, P. R., V. Cristofoletti, and N. Romeo. 1978. A band model for melanin deduced from optical absorption and photoconductivity experiments. *Biochim. Biophys. Acta.* 538:164–170.

49. Wolbarsht, M. L., A. W. Walsh, and G. George. 1981. Melanin, a unique biological absorber. *Appl. Opt.* 20:2184–2185.

50. Nemkovich, N. A., A. N. Rubinov, and V. I. Tomin. 1991. Inhomogeneous broadening of electronic spectra of dye molecules in solutions. *Top. Fluoresc. Spectrosc.* 2:367–428.

51. Vitkin, I. A., J. Woolsey, B. C. Wilson, and R. R. Anderson. 1994. Optical and thermal characterization of natural (*sepia officinalis*) melanin. *Photochem. Photobiol.* 59:455–462.

52. Sardar, D. K., M. L. Mayo, and R. D. Glickman. 2001. Optical characterization of melanin. *J. Biomed. Opt.* 6:404–411.

53. Huang, J. S., J. Sung, M. Eisner, S. C. Moss, and J. Gallas. 1988. The fractal structure and the dynamics of aggregation of synthetic eumelanin in low pH aqueous solutions. *J. Chem. Phys.* 90:25–29.

54. Kurtz, S. K. 1986. Light scattering calculations for melanin pigments from the Rayleigh to the Mie regime. *J. Investig. Derm.* 87:400–401.

55. Nighswander-Rempel, S., J. Riesz, J. Gilmore, J. Bothma, and P. Meredith. 2005. Quantitative fluorescence excitation spectra of synthetic eumelanin. *J. Phys. Chem. B.* 109:20629–20635.

56. Damjanovic, A., H. M. Vaswani, P. Fromme, and G. R. Fleming. 2002. Chlorophyll excitations in photosystem I of synechococcus elongatus. *J. Phys. Chem. B.* 106:10251–10262.